AD-A283 198

UMENTATION PAGE

Form Approved
OMB No. 0704-188

ORT DATE	3. REPORT TYPE AND DATES COVERED
June 1994	FINAL

4. TITLE AND SUBTITLE
Direct measurements of edge diffraction from soft underwater acoustic panels

5. FUNDING NUMBERS
PE - 61153N
TA - RR011
WU - DN220-161

6. AUTHOR(S)
Jean C. Piquette

7. PERFORMING ORGANIZATION NAME(S) AND ADDRESS(ES)
NAVAL RESEARCH LABORATORY
UNDERWATER SOUND REFERENCE DETACHMENT
P.O. BOX 568337
ORLANDO, FL 32856-8337

8. PERFORMING ORGANIZATION REPORT NUMBER

9. SPONSORING/MONITORING AGENCY NAME(S) AND ADDRESS(ES)
OFFICE OF NAVAL RESEARCH
800 N. QUINCY ST.
ARLINGTON, VA 22217-5000

10. SPONSORING/MONITORING AGENCY REPORT NUMBER

11. SUPPLEMENTARY NOTES
Published in JASA 95 (6), pp. 3090-3099, June 1994.

12a. DISTRIBUTION/AVAILABILITY STATEMENT
Approved for public release; distribution unlimited.

12b. DISTRIBUTION CODE

13. ABSTRACT *(Maximum 200 words)*

Direct measurements of edge diffraction arising from the interaction of an acoustic wave with an underwater panel that satisfies soft-body boundary conditions are reported. The measurements were obtained by utilizing a specially fabricated "airbox" sample, which is literally a "box of air," fabricated using thin polycarbonate walls. The airbox theoretically would exhibit a typical insertion loss in excess of 60 dB (in the absence of edge diffraction), thus avoiding interference of the directly transmitted wave with the edge-diffracted wave of interest. The validity of the edge-diffraction measurements was established by demonstrating that the performance of a small sample panel fabricated from a closed-cell foam material can be deduced by adding (frequency-by-frequency) measurements obtained from an airbox to diffraction-free measurements obtained from a large sample of the same closed-cell foam. This procedure simulates (from direct experimental measurements) the combined edge-diffracted plus transmitted wave field that is present in the transmission region of the small sample. The results reported include the edge diffraction caused by the interaction of a spherically symmetric source with a soft sample panel and the edge diffraction caused by the interaction of an acoustic array with a soft sample panel. The frequency interval considered is 1-21 kHz.

14. SUBJECT TERMS
Diffraction, Edge diffraction, Panel tests, Insertion loss, Echo reduction, Transient suppression

15. NUMBER OF PAGES
10

16. PRICE CODE

17. SECURITY CLASSIFICATION OF REPORT	18. SECURITY CLASSIFICATION OF THIS PAGE	19. SECURITY CLASSIFICATION OF ABSTRACT	20. LIMITATION OF ABSTRACT
UNCLASSIFIED	UNCLASSIFIED	UNCLASSIFIED	SAR

Vol. 95, No. 6, June 1994

Direct measurements of edge diffraction from soft underwater acoustic panels

Jean C. Piquette
Naval Research Laboratory, Underwater Sound Reference Detachment, Orlando, Florida 32856-8337

pp. 3090-3099

Direct measurements of edge diffraction from soft underwater acoustic panels

Jean C. Piquette
Naval Research Laboratory, Underwater Sound Reference Detachment, Orlando, Florida 32856-8337

(Received 15 July 1993; accepted for publication 23 January 1994)

Direct measurements of edge diffraction arising from the interaction of an acoustic wave with an underwater panel that satisfies soft-body boundary conditions are reported. The measurements were obtained by utilizing a specially fabricated "airbox" sample, which is literally a "box of air," fabricated using thin polycarbonate walls. The airbox theoretically would exhibit a typical insertion loss in excess of 60 dB (in the absence of edge diffraction), thus avoiding interference of the directly transmitted wave with the edge-diffracted wave of interest. The validity of the edge-diffraction measurements was established by demonstrating that the performance of a small sample panel fabricated from a closed-cell foam material can be deduced by adding (frequency-by-frequency) measurements obtained from an airbox to diffraction-free measurements obtained from a large sample of the same closed-cell foam. This procedure simulates (from direct experimental measurements) the combined edge-diffracted plus transmitted wave field that is present in the transmission region of the small sample. The results reported include the edge diffraction caused by the interaction of a spherically symmetric source with a soft sample panel and the edge diffraction caused by the interaction of an acoustic array with a soft sample panel. The frequency interval considered is 1–21 kHz.

PACS numbers: 43.20.Gp, 43.40.Le, 43.40.Rj

INTRODUCTION

Panel measurements are a standard method whereby the behavior of passive acoustical materials intended for underwater applications is determined. (The reader unfamiliar with underwater panel measurement methodology should refer, e.g., to Refs. 1 and 2.) One difficulty that arises in underwater panel measurements is the interfering influence of the edge-diffracted wave; in an insertion-loss measurement, this is the wave that passes around, rather than through, the panel. (A similar edge-diffracted wave appears in an echo-reduction measurement.) The edge-diffraction problem is particularly severe in insertion-loss measurements performed on samples fabricated from soft materials for two reasons. First, such samples often exhibit a large insertion loss (40 dB or more is not unusual), even at rather low frequencies (below 5 kHz). Thus the amplitude of the directly transmitted wave can become rather small, and can even fall below the amplitude of the edge-diffracted wave. The second problem arises from the very low sound speed characteristic of soft materials. This sound speed is typically less than the speed of sound in air, and may even be less than one half the speed of sound in air. Such very low speeds often preclude the possibility of separating the directly transmitted and edge-diffracted waves based on their differing times of flight. Indeed, for a typical panel of 76.2 cm $\times$ 76.2 cm lateral dimensions, even a sample having a sound speed equal to that of air and a thickness of 3 cm would have its first multiple internal reflection contribute to the transmitted wave after the arrival of the edge-diffracted wave, assuming plane-wave insonification. Since contributions from several internal reflections often must occur before the directly transmitted wave satisfactorily approximates steady-state conditions, it is important to determine the strength of the edge-diffracted wave arising in such measurements.

Relatively little experimental work[3–5] has been done previously on this problem, with the majority of previous work being theoretical and/or numerical in character.[6–8] Most of this previous work has not focused on soft panels, with the notable exception of the work of Radlinski.[7,8]

In the present work, a method for directly observing the edge-diffracted wave from a soft body fabricated into the shape of a panel is described. The approach is based on measurements from an "airbox" sample. (The airbox is an experimental approximation to an ideal soft body having the same geometry as a sample panel of interest.) By adding airbox measurements to diffraction-free measurements obtained from a penetrable foam sample of large lateral dimensions, it is shown that the performance of a small sample fabricated from the same foam material can be deduced. (The summation of these two experimental wave-fields simulates the combined edge-diffracted plus directly transmitted wave-field components that are simultaneously present in the transmission region of the small sample.) This procedure thus verifies the validity of using the airbox measurements as a method for observing edge diffraction in soft-panel measurements.

The airbox is fabricated from polycarbonate sheet material of 0.64 cm thickness. The sample is literally a "box of air," whose interior dimensions are 76.2 cm $\times$ 76.2 cm $\times$ 2.54 cm in order to simulate the geometry of a sample of interest. The wave directly transmitted through the airbox (in the absence of edge waves) has a theoretical amplitude typically 60 dB below that of the interrogating wave, thus

providing very little interference with the measurement of the edge-diffracted wave of interest.

The validity of using the airbox measurements as a method for directly observing the edge-diffracted wave is established by comparison with measurements obtained from samples fabricated from a commercially available closed-cell foam material, Microcell™, manufactured by Sentinel Products of Hyannis, MA. The Microcell selected for use had a nominal density of 0.16 g/cm^3 (10 lb/ft^3). (Measurements on small pieces of the Microcell used showed density variations of ±5% about the nominal value.) Two sample panels of this material were fabricated. One sample (the "small sample") was fabricated with the same geometry as the air-containing region of the airbox. The second sample (the "large sample") was fabricated with dimensions 229 cm × 229 cm × 2.54 cm. (The large sample was fabricated by bonding together nine small samples in a 3 × 3 array, much like the array of squares in tic-tac-toe. The central element of this array was left unbonded, so that it could be removed and also serve as the small sample.)

Measurements made in the transmission region of the *small* sample contain two wave-field components: (i) the directly transmitted wave plus (ii) the edge-diffracted wave. By using an appropriate measurement "gate" during data acquisition from the *large* sample, only directly transmitted wave data are obtained. The equivalence of the edge-diffraction *component* of the small-sample measurement to the edge diffraction obtained from the airbox measurement is established by computing (from direct experimental measurements) *simulated* small-sample measurements. These simulated small-sample measurements are computed by forming the frequency-by-frequency complex sum of the large-sample measurements (which simulate only the directly transmitted component of the small-sample results) plus the airbox measurements (which simulate only the edge-diffracted component of the small-sample results). The magnitudes of these simulated small-sample results are shown to agree reasonably well with the magnitudes of the directly observed small-sample measurements.

Section I describes the measurement setup. In Sec. II, the results of the airbox measurements are presented. In Sec. III, the results of the Microcell measurements are presented. Section IV gives a discussion of the results. Finally, a summary and the conclusions are given in Sec. V.

I. MEASUREMENT RIG AND SAMPLE HOLDERS

A special test rig and special sample holders were fabricated to obtain the measurements [see Fig. 1(a)–(c)]. The measurements were obtained in the Lake Facility (LAFAC) of the Underwater Sound Reference Detachment of the Naval Research Laboratory (NRL-USRD) in Orlando, FL. The rig was designed to allow the samples to be positioned in a horizontal plane while submerged. This was found to be necessary during earlier measurement attempts in which it was found that the large sample suffered substantial warping due to the influences of hydrostatic pressure gradients when held in a vertical orientation. The rig design allows for vertical orientation when the rig is placed on the deck of the facility pier, for ease in changing samples and acoustical elements. The rig also contains quick-release clamps around its periphery (i.e., outside the acoustic field) for ease of securing and removing samples from the rig.

Each of the three samples of interest, i.e., the airbox, the large sample, and the small sample, has its own specially designed sample holder (note again Fig. 1). Each sample holder includes a frame fabricated from 2.54 cm × 7.62 cm (1 in × 3 in) aluminum bar stock. These aluminum frames have outside dimensions of 244 cm × 244 cm, so all the aluminum lies outside the acoustic field. (It is the aluminum frame of each sample holder which the quick-release clamps of the main rig secure in place.) The Microcell samples are held in each sample-holder frame in much the same way as a picture is held in a picture frame. The large-sample holder also includes two polycarbonate support sheets of 244 cm × 244 cm × 0.64 cm dimensions, with one sheet located on either side of the aluminum frame, to help secure the large sample in place. Rubber washers are used to form an offset region between the aluminum frame and each polycarbonate support sheet so that the frame free floods when submerged.

The small-sample and airbox holders each contain only a single polycarbonate support sheet of 244 cm × 244 cm × 0.64 cm dimensions. This is possible because the horizontal orientation of the rig during submergence allows the effects of hydrostatic pressure gradients, i.e., buoyancy, to hold the sample securely against the single polycarbonate support sheet. [Note in Fig. 1(a) that the airbox is situated *beneath* the polycarbonate support sheet when the rig is oriented horizontally; the small sample also is situated below its polycarbonate support sheet when the rig is in this orientation.] Care is taken to exclude any trapped air between each Microcell sample and its support sheet. The airbox is secured to its polycarbonate support sheet using nylon screws and cyanoacrylate adhesive. (The polycarbonate support sheet used in the airbox holder actually serves to form the back surface of the airbox, thus reducing the total amount of plastic in the acoustic field.) Finally, the small sample is held at the center of its polycarbonate support sheet by eight small polycarbonate blocks located at the periphery of the small sample [see Fig. 1(c)]. (When the small sample is not submerged, it is held in place by friction with the small polycarbonate blocks; when submerged, buoyancy holds the small sample against the large polycarbonate support sheet.) The small blocks are held to the support sheet with nylon screws, and are designed to allow a small offset region between the small sample and its support sheet so that the holder free floods when submerged.

During insertion of each sample into the facility pool, the rig is rotated into the horizontal position. This rotation is accomplished through the use of two rigging hoists which are attached by cables to the main rig as shown in Fig. 1(a). By raising one cable while lowering the other, the sample can be rotated through the necessary 90°. The physical pendulum formed by the rig, the sample, and the

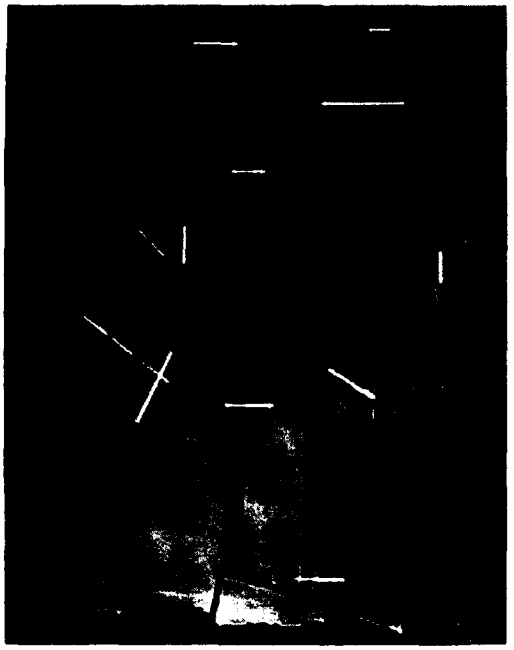

(a)

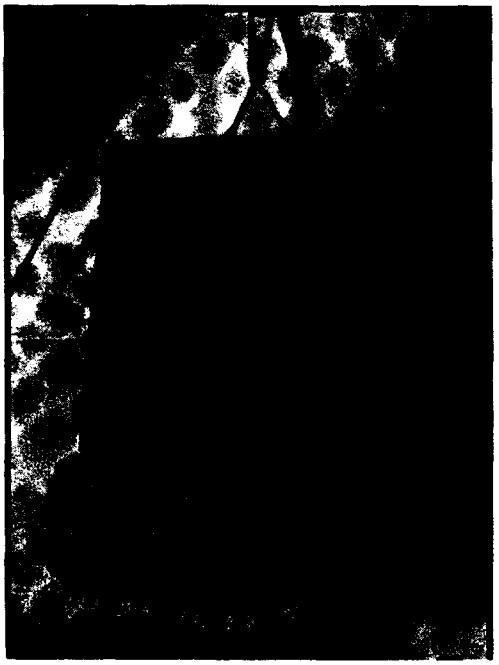

(b)

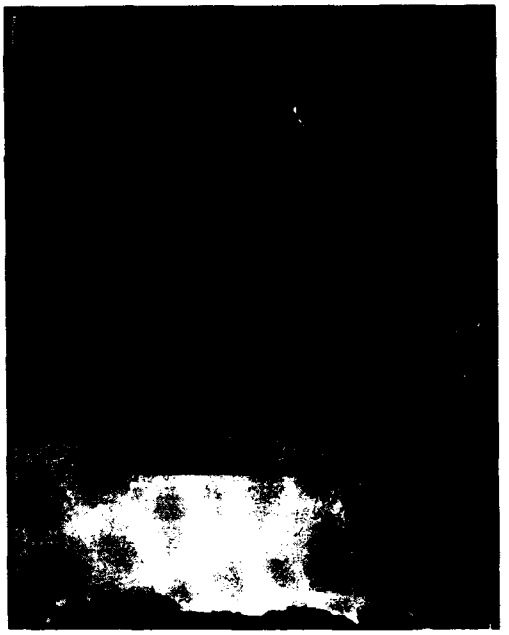

(c)

FIG. 1. The measurement rig and samples situated in their relevant sample holders. The rig and sample holders are shown suspended in midair from the pier superstructure. (a) Measurement rig depicted in the horizontal orientation. Airbox sample is shown clamped in place in the rig. (b) "Large sample" of 229 cm × 229 cm × 2.54 cm dimensions depicted within its sample holder. (c) "Small sample" of 76.2 cm × 76.2 cm × 2.54 cm dimensions depicted within its sample holder. Note the eight polycarbonate support blocks that can be seen around the periphery of the sample.

hoist-cable suspension is stable in all planes of rotation. Hence, when the system is suspended in the horizontal position and disturbed, restoring forces cause it to return to the horizontal position. Similar restoring forces cause the system to remain in the vertical position when suspended in that fashion.

II. AIRBOX MEASUREMENTS

All measurements reported here utilized either an F56 projector[9] or an F43 projector[10] as a sound source. The source-to-panel offset used was 150 cm. An H52 hydrophone[9] was used for signal detection. The F56 projector is a piezoelectric spherical shell that approximates the behavior of a point source below the device's lowest resonance frequency of about 12 kHz. The F43 is an array of piezoelectric tubes, useful as a projector in the frequency range 1–21 kHz. For frequencies above about 5 kHz, the F43 has a primary beamwidth of less than 60°, and acts largely as a plane-wave source within the primary beam. Below about 5 kHz the F43 loses much of its directionality, and behaves largely as a point source.

In order to reduce the influences of the turn-on transients of the projectors on the results, the projectors were each driven in the transient-suppressed mode.[11,12] A typical directly radiated transient-suppressed waveform produced by the F56 at 10 kHz is shown in Fig. 2(a). (The data window depicted here, and in subsequent figures, was selected to avoid rigging reflections.) As can be seen, the turn-on transient is only of about one cycle duration. After interaction of this waveform with the airbox sample, the

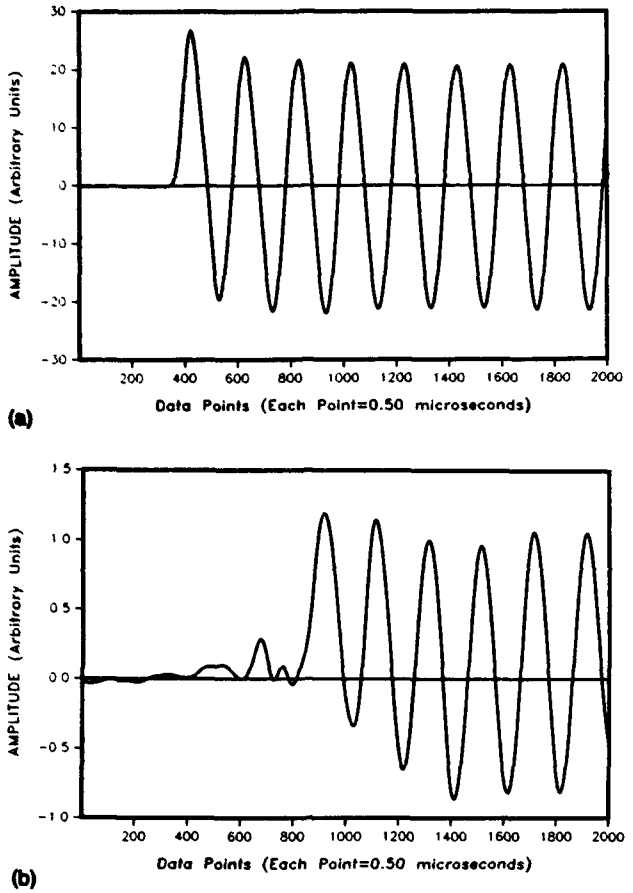

FIG. 2. F56 transient-suppressed waveforms at 10 kHz. (a) Directly radiated waveform. This waveform was captured with the hydrophone situated at the nominal 5-cm offset position; however, the sample was removed. (b) Edge-diffracted waveform, resulting from the interaction of the waveform of Fig. 2(a) with the airbox sample.

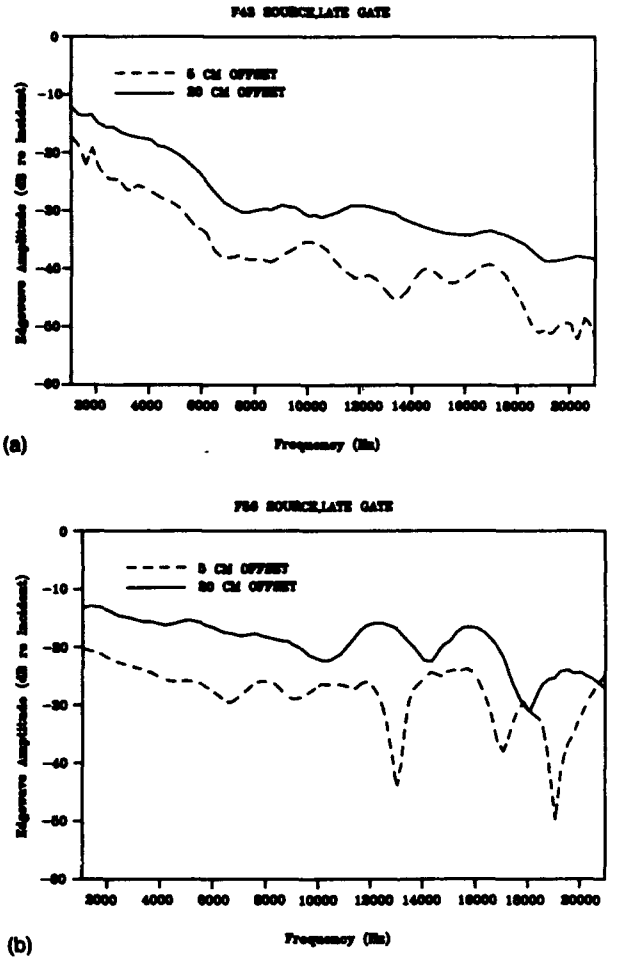

FIG. 3. Airbox edge diffraction. Solid line: 20-cm hydrophone offset. Dashed line: 5-cm hydrophone offset. (a) F43 source. (b) F56 source.

resulting waveform is depicted in Fig. 2(b). As can be seen, the transient region of the observed waveform is of considerably greater duration compared with that of the interrogating waveform, because of the extended size of the sample, with steady-state conditions not occurring until perhaps the last two cycles depicted. During the subsequent frequency sweeps that were performed, amplitude levels were determined by gating on the last available full cycle prior to the reception of rigging reflections, while maintaining a one-cycle gate width at each test frequency. (In the low-frequency interval 1 to 3 kHz, a fractional-cycle window width was used. At 1 kHz, a $\frac{1}{2}$-cycle window width was used and at 3 kHz a 1-cycle window width was used. Between 1 and 3 kHz, the window width was varied linearly between the $\frac{1}{2}$-cycle and 1-cycle endpoint widths. Wave amplitude within the window was determined by least-squares fitting to a sine wave at each test frequency.)

It is worth mentioning that the F56 turn-on transient caused by a *gated-sine* drive voltage is of about 4 cycles duration at 10 kHz. Hence, if transient-suppressed interrogating waves were not used, the steady state of the edge-diffracted wave would not have occurred prior to the arrival of rigging reflections in the setup that was used.

Sweeps of edge-diffraction levels are shown in Fig. 3(a) and (b). (The vertical axis in this figure represents the edge-wave amplitude in decibels *re* the incident-wave amplitude at the hydrophone position when the sample is absent. This is the negative of the result that would be obtained in an insertion-loss calculation. This manner of presenting the results is chosen so that large edge-wave amplitudes produce values that are high on the vertical axis, and small edge-wave amplitudes produce values that are low on the vertical axis. This is similar to the manner of presenting results used by Radlinski.[7,8]) The term "late gate" in these, and subsequent, figures denotes that the measurement gate has been set to avoid rigging reflections in the manner discussed above. (It should be understood that the rig is submerged in the facility pool at a depth such that setting the gate to avoid rigging reflections also avoids lake surface and bottom reflections.) In Fig. 3(a) is shown the edge-diffraction amplitude for the F43 source and in Fig. 3(b) is shown the edge-diffraction amplitude for the F56 source. Solid lines show results for a 20-cm hydrophone-to-panel offset distance and dashed lines show results for a 5-cm hydrophone-to-panel offset distance. As should be expected, the larger offset distance produces generally higher-amplitude edge-diffracted waves. It is also worthwhile noting that edge diffraction from the F56 source is of generally greater amplitude than that from the

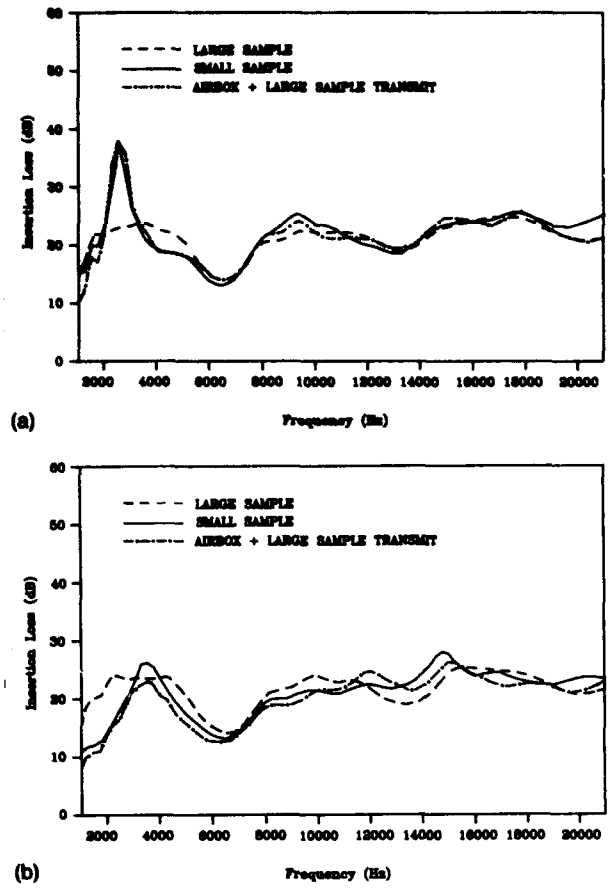

FIG. 4. Microcell insertion loss sweeps for the F43 source. Solid line: small sample. Dashed line: large sample. Dot–dashed line: magnitude of the sum of the complex large-sample amplitude plus the complex airbox amplitude relative to the incident wave. (a) 5-cm hydrophone offset. (b) 20-cm hydrophone offset.

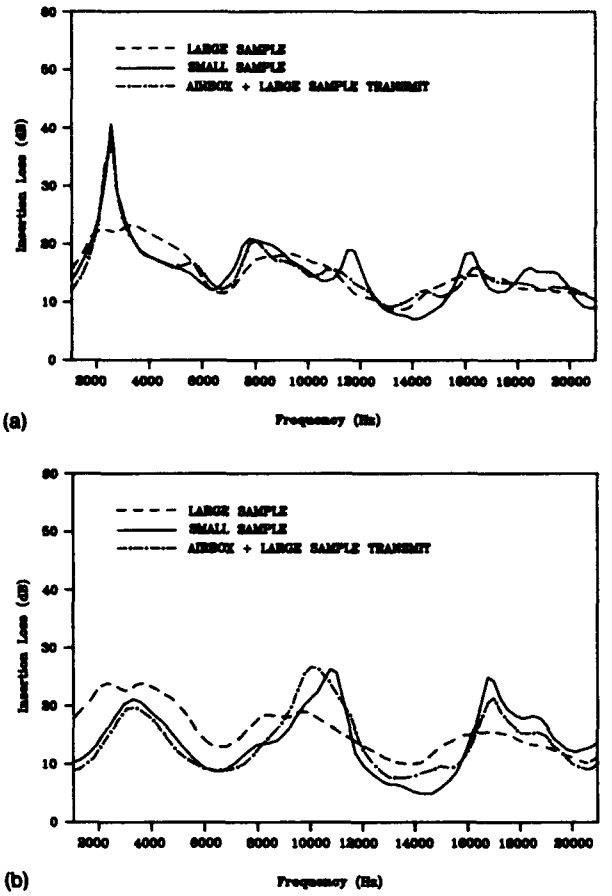

FIG. 5. Microcell insertion loss sweeps for the F56 source. Solid line: small sample. Dashed line: large sample. Dot–dashed line: magnitude of the sum of the complex large-sample amplitude plus the complex airbox amplitude relative to the incident wave. (a) 5-cm hydrophone offset. (b) 20-cm hydrophone offset.

F43 source, as should be expected in view of the directionality of the F43. At lower frequencies the results for the two sources become similar, reflecting the fact that the F43 loses its directionality at low frequency.

It is worthwhile noting that the actual hydrophone-to-panel offset distance must be experimentally determined. The 5- and 20-cm nominal offsets as initially positioned are not the correct offsets for three reasons. First, the offset is measured with respect to the polycarbonate surface of the airbox, thus requiring the addition of the 0.64-cm plastic thickness to the nominal offset. Second, the polycarbonate support sheet is not entirely rigid, and hence permits the airbox to float up and somewhat increase the hydrophone-to-panel separation. (Recall that the sample is positioned horizontally during acoustic testing.) Third, the rigging pole used to position the H52 hydrophone is not perfectly rigid and bends slightly under gravity, further increasing the offset. Thus the correct hydrophone-to-panel offset must be experimentally determined. This determination was made with the help of an underwater video camera. (The measurement required affixing a plumb line with a reference length scale to the airbox.) The measured offset from the air-containing region of the airbox to the hydrophone while the sample was submerged with the rig in the horizontal orientation was 8.3 cm, indicating a 3.3-cm difference from the nominal 5-cm offset.

By assuming the same 3.3-cm difference in offset at the 20-cm nominal hydrophone position, we obtain an actual hydrophone position of 23.3 cm. By running the software described in Ref. 4, a *qualitative* idea of the expected edge-wave level for the measurement can be deduced. (This software computes edge levels for a circular disk, so quantitative agreement is not expected. However, the differences for the two geometries should be smaller the lower the frequency considered. The disk diameter was taken to be equal the edge length of the airbox.) Running a circular-disk calculation for the actual hydrophone offsets and the 1-kHz test frequency yields a computed value of edge diffraction of -20.3 dB for the smaller of the two offsets and -12.5 dB for the larger of the two offsets. The observed value for the smaller offset, which can be read from the dashed-line curve presented in Fig. 3(b), is about -20.1 dB. The observed value for the larger offset, which can read from the solid-line curve of Fig. 3(b), is about -12.9 dB. The agreement of the experimental and theoretical values of edge diffraction provides some indication of the validity of the measurements.

III. MICROCELL MEASUREMENTS

Figures 4(a) and (b) and 5(a) and (b) present

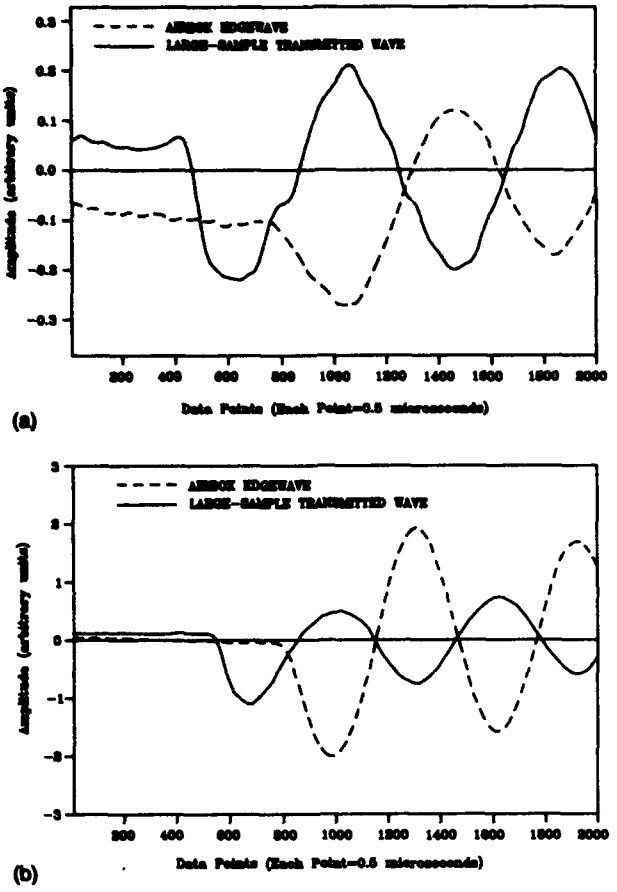

FIG. 6. Airbox edgewaves compared with large-sample transmitted waves. Solid line: large sample transmitted wave. Dashed line: airbox edge wave. (a) F43 source, 5-cm hydrophone offset, 2.5 kHz. (b) F56 source, 20-cm hydrophone offset, 3.25 kHz.

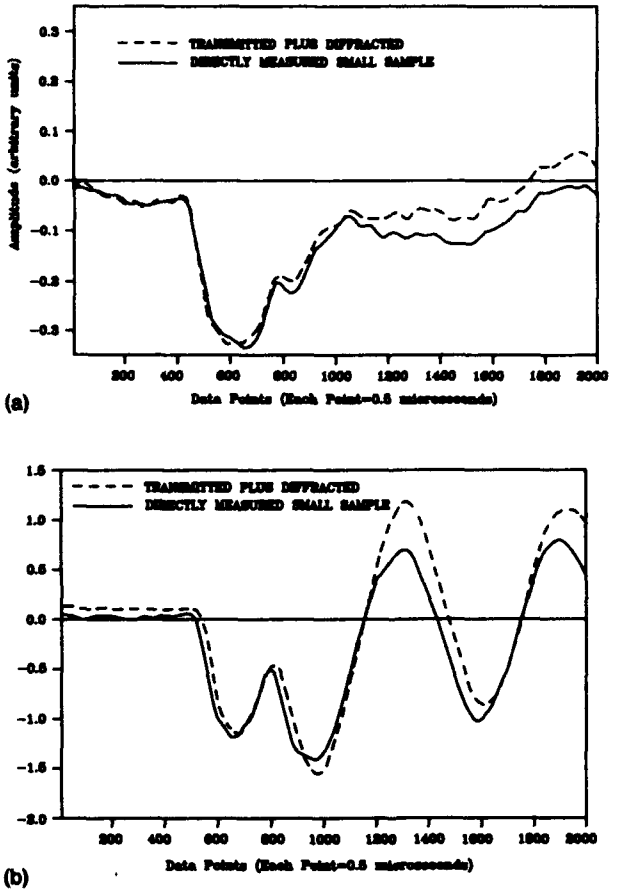

FIG. 7. Sum of large-sample transmitted wave plus airbox-diffracted edge wave compared with directly measured small-sample wave. Solid line: directly measured small-sample wave. Dashed line: sum of large-sample transmitted wave plus airbox edgewave. (a) F43 source, 5-cm hydrophone offset, 2.5 kHz. (b) F56 source, 20-cm hydrophone offset, 3.25 kHz.

insertion-loss sweeps obtained from the Microcell samples. (These figures also each contain a curve that includes combined Microcell and airbox data, denoted by the dot–dashed line. These combined data will be discussed presently.) Differences between the large- and small-sample results are attributed primarily to the influences of edge diffraction. It was determined that negligible sound leakage was occurring through the seams in the large Microcell sample from the fact that the insertion loss for each of the two hydrophone offsets considered differ only very slightly. [Compare the dashed-line curve of Fig. 4(a) with that of Fig. 4(b), and of Fig. 5(a) with Fig. 5(b).] Seam-leakage wave amplitudes would be expected to behave similarly to edge diffraction, and hence to vary substantially with hydrophone offset, owing to the significantly different aspect angle from seam-to-hydrophone for each offset. That is, seam-leakage waves would be expected to vary with a behavior similar to that seen for the edge-diffraction levels depicted for each of the two hydrophone offsets considered in Fig. 3(a) and (b). This expectation is substantiated by the large variations seen in the *small*-sample insertion-loss curves for each of the two offsets; compare the solid-line curve of Fig. 4(a) with that of Fig. 4(b), and of Fig. 5(a) with Fig. 5(b). The rather negligible changes in the large-sample insertion-loss curves of Figs. 4 and 5 between the two hydrophone offsets clearly suggest no significant seam-leakage waves were present in these measurements.

If the wave diffracted by the airbox edge is in fact equivalent to that diffracted by the small-sample edge, it should be possible to deduce the small-sample results by adding the airbox results to the large-sample results. This follows from the expectation that the small-sample results are, in fact, the combination of the directly transmitted wave (which is essentially all that is present in the large-sample measurement) plus the edge-diffracted wave (which is essentially all that is present in the airbox measurement).

This idea is examined for the time domain in Figs. 6(a) and (b) and 7(a) and (b). In Fig. 6, digitized waveforms acquired in the airbox measurement are compared with digitized waveforms acquired in the large-sample measurement. Figure 6(a) presents the case of the F43 source with a 5-cm hydrophone offset and a test frequency of 2.5 kHz, while Fig. 6(b) presents the case of the F56 source with a 20-cm hydrophone offset and a test frequency of 3.25 kHz. We examine these particular frequencies in each case because the small-sample measurements each exhibit pronounced, isolated, insertion-loss peaks for these frequencies while the large-sample measurements do

not [examine, again, Fig. 4(a) and Fig. 5(b)]. These pronounced peaks in the small-sample insertion-loss curves arise from the presence of an edge-diffracted wave that is close in amplitude to the directly transmitted wave, but 180° out of phase with it. This behavior can clearly be seen in Fig. 6(a) and (b). (Of course, the edge-diffraction interference which causes the peaks in the *small-sample* insertion-loss curves is being evaluated here by examining waveforms acquired from the *airbox*.)

The validity of the idea that the small-sample performance can be deduced by adding airbox and large-sample measurements is further shown for the time domain by the results presented in Fig. 7(a) and (b). Here, the result of the direct point-by-point summation of the digitized, large-sample transmitted wave plus the digitized airbox edge-wave is compared with the directly measured digitized small-sample wave. [The parameters considered in Fig. 7(a) and (b) are the same, respectively, as those considered in Fig. 6(a) and (b).] As can be seen, the computed and directly measured waves are in reasonably good agreement.

By examining Fig. 7(a) and (b), one can see that the discrepancies increase as a function of increasing time. While the reasons for this behavior are not exactly known, some reasonable possibilities can be suggested. Recall that the waveforms of Fig. 7(a) and (b) correspond to points of maximum interference on the small-sample insertion-loss graphs of Figs. 4(a) and 5(b), respectively, i.e., to points of maximum cancellation of the directly transmitted and edge-diffracted waves. Since these two wave-field components are the strongest contributing components to the data, their mutual cancellation would tend to emphasize the presence of any coherent noise. Such coherent noise could arise partly from seam-leakage waves in the large sample; although such waves are of generally negligible amplitude, their presence would be most apparent when the directly transmitted and edge-diffracted waves cancel each other. Furthermore, recall that the central element of the large-sample matrix is the small sample itself. For times during which only arrivals of the large-sample transmitted wave that have passed through the central matrix element contribute to the observations, agreement of the curves of Fig. 7(a) and (b) would be expected to be best. At later times, when arrivals from the large-sample transmitted wave which have passed through the outer matrix elements contribute to the observations, agreement would be expected to decrease (recall the density variations in the Microcell samples used). This behavior is consistent with that seen in Fig. 7(a) and (b).

The notion that the small-sample results can be deduced by summing the airbox and large-sample results is substantiated, in the frequency domain, for the entire frequency interval measured in the present experiment, by the dot–dashed curves presented in Figs. 4(a) and (b) and 5(a) and (b). Compare the directly measured small-sample insertion loss in these figures (solid-line curves) with the effective insertion loss determined by summing, frequency-by-frequency, the large sample and airbox complex amplitude measurements (dot–dashed curves). The insertion loss is determined in the effective cases using the ordinary formula (which compares the measurement to the amplitude of the incident wave) for this calculation. The dot–dashed curves of Fig. 4(a) and (b) present results for the F43 source while those of Fig. 5(a) and (b) present results for the F56 source. As can be seen, the directly measured and effective (or synthetic) insertion-loss curves are in reasonably good agreement across the frequency interval considered. Although the agreement is imperfect, the dot–dashed curves clearly track the solid-line curves of Figs. 4(a) and (b) and 5(a) and (b) far better than do the dashed-line curves, indicating that the airbox edge-diffraction measurements have accounted for the majority of the differences between the large- and small-sample measurements.

The dot–dashed curves of Figs. 4 and 5 should also be compared with the dashed-line curves of these figures, in order to see how much the large-sample results are modified by the addition of the airbox results in bringing the large-sample curves into agreement with the small-sample curves. The most significant effects are seen in Fig. 5(b), the case of the 20-cm hydrophone offset for the F56 source.

IV. DISCUSSION

The case involving the F43 source and 5-cm hydrophone-to-panel offset distance is of special interest, since this setup approximates that used in panel measurements as performed in the Anechoic Tank Facility located at NRL-USRD. However, if desired, the same experimental setup ought to be useful for determining the validity of measurement methods based on other geometries, such as those that utilize a receiving array,[8] rather than the H52 "point" hydrophone considered here.

Although the typical edge-diffraction level observed here for the F43 source and 5-cm hydrophone-to-panel offset falls below about −40 dB for frequencies above about 12 kHz, this level is nonetheless significant in many measurements of interest. For example, a sample characterized by a 30-dB insertion loss can be inaccurately measured to an error of greater than 3 dB if the phasing of the directly transmitted and edge-diffracted waves is unfavorable. Note, for example, the approximately 2-dB error at about 9.5 kHz in Fig. 4(a) between the large- and small-sample curves. The edge-wave level for this case is about −36 dB [note Fig. 3(a), dashed line], while the insertion loss of interest is about 21 dB [note Fig. 4(a), dashed line]. Approximately 1.7 dB of the observed 2-dB error can be explained by assuming that the edge-wave arrives at the detector 180° out of phase with the directly transmitted wave in this measurement. This assumption is consistent with the fact that the small-sample insertion loss [Fig. 4(a), solid line] *exceeds* the insertion loss of the large sample [Fig. 4(a), dashed line] at this frequency.

It has been remarked previously that the airbox exhibits a *typical* insertion loss exceeding 60 dB in the absence of edge waves. However, a laterally infinite layer of air of 2.54 cm thickness would be expected to exhibit thickness resonances at frequencies 6.5, 13.0, and 19.5 kHz in the frequency band of interest. At these frequencies such a layer

of air would exhibit essentially *zero* insertion loss. The experimental data exhibit very little evidence of the presence of such resonances. This may be due to the fact that the polycarbonate used to fabricate the airbox may introduce sufficient loss into the system to eliminate, or greatly reduce, the influences of these resonances. On the other hand, the pronounced peaks in the dashed-line curve of Fig. 3(b) near 13 and 19 kHz might be attributable to this cause. Such an explanation, however, is difficult to reconcile with the virtual absence of these peaks in the curves of Fig. 3(a) (with the exception of the minor peak near 13 kHz, despite the generally lower edge-wave level evident in these curves, and is also difficult to reconcile with the apparent presence of these peaks in the *solid*-line curve of Fig. 3(b), at shifted frequencies, where the edge-wave level is of significantly greater amplitude. Such an explanation would also fail to account for the peak in the dashed-line curve of Fig. 3(b) in the vicinity of 17 kHz. Also, the relatively constant gap between the solid-line and dashed-line curves of Fig. 3(a) and (b) over much of the frequency interval is reasonable provided that only an edge-diffracted wave of significant amplitude is present in the measurement, and is rather incompatible with the presence of a transmitted wave of substantial amplitude. Nonetheless, *some* of the variations in the curves of Fig. 3(a) and (b) are probably attributable to the presence of an airbox transmitted wave of nonzero amplitude.

It is also worthwhile to discuss the idea that the influences of edge diffraction reported here might be avoided by a judicious placement of the data-acquisition gate. That is, it is certainly possible, in principle, for the samples considered here to set the data-acquisition gate to avoid entirely the contribution of the edge-diffracted wave to the observed signal. Although the source turn-on transient often precludes such a strategy, the use of transient-suppressing drives might be thought to make possible a proper gating strategy that avoids edge diffraction. Unfortunately, since the steady-state wave that is transmitted through the panel includes multiple contributions from *internal* reflections, the steady-state condition usually requires a buildup time that exceeds the measurement time available prior to the reception of edge diffraction. This idea is examined for the frequency domain in Fig. 8, in which insertion-loss measurements utilizing an "early gate" are compared with insertion-loss measurements utilizing a "late gate" for the *large* sample. (The early gate avoids the edge diffraction that would be present if the measurement were being performed on the small sample, and hence *simulates* an edge-diffraction-free small-sample measurement, and the late gate avoids rigging reflections.) As can be seen, the two curves differ significantly, illustrating the fact that multiple internal echoes have not contributed to the early-gate measurements. (Note that the "waviness" of the late-gate insertion-loss curve might erroneously be assumed to be attributable to edge diffraction, possibly inducing a panel-measurement system operator to mistakenly use an early-gate setting when, in fact, this waviness is actually due to thickness resonances in this sample.)

The notion that multiple internal reflections contribute

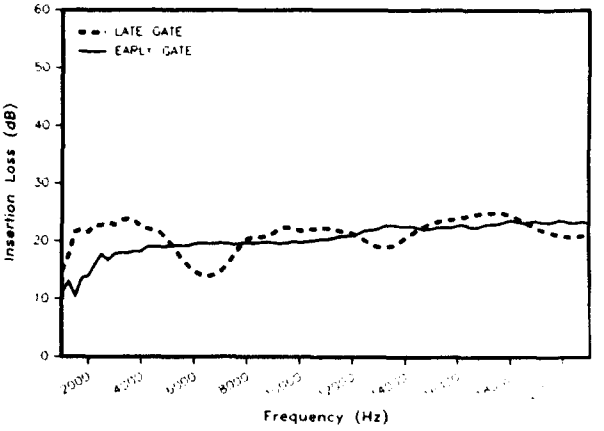

FIG. 8. Large-sample insertion loss for the F43 source and 5-cm offset. Solid line: early gate, i.e., the measurement gate is set such that it would avoid edge diffraction if the measurement were being performed on the small sample. Dashed line: late gate, i.e., the measurement gate is set to avoid rigging reflections.

significantly to the steady-state transmitted-wave amplitude is further substantiated for the time domain by the waveforms presented in Fig. 9(a) and (b). In Fig. 9(a) is presented a transient-suppressed single-cycle interrogating

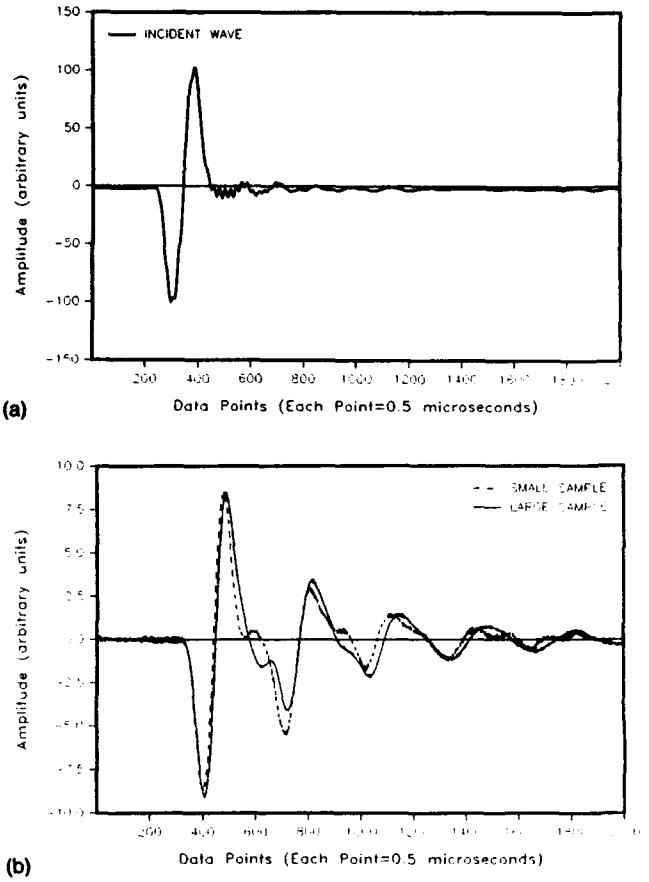

FIG. 9. Single-cycle transient-suppressed interrogating waveform from the F43 source at 12-kHz and wave train resulting from sample interaction. (a) Interrogating, or incident, single-cycle waveform. (b) Resulting wave train, as seen on the transmission side of the sample, when the waveform of (a) interacts with either the large sample or the small sample. Solid line: large sample. Dashed line: small sample.

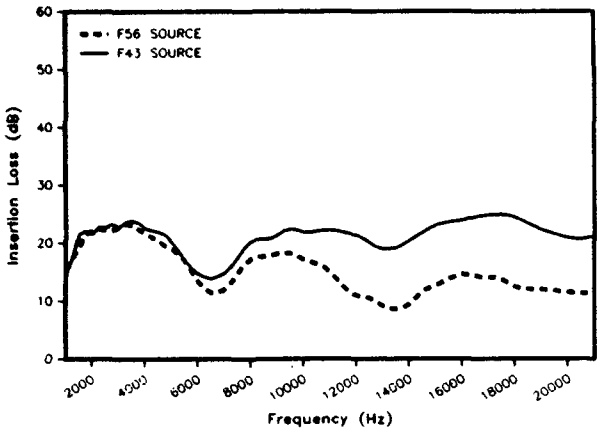

FIG. 10. Large-sample insertion loss for the F56 compared with that for the F43. Dashed line: F56 source. Solid line: F43 source.

waveform of 12 kHz center frequency for the F43 source. The resulting wave train that arises when this waveform interacts with either the small or large sample is presented in Fig. 9(b). The multiple internal contributions are apparent. Dispersion effects can also be seen in that higher-order multiple internal reflections exhibit significantly modified wave shape with respect to the interrogating waveform (i.e., waveform spreading can be seen).

Finally, it is worthwhile noting that the insertion-loss measurements using the F43 source differ significantly from those obtained using the F56 source, even in the large-sample cases, especially at the upper end of the frequency interval considered (see Fig. 10). This result is qualitatively consistent with the theoretical expectation[13,14] that the transmitted-wave amplitude for spherical-wave excitation can be generally significantly greater than for plane-wave excitation.[15–17] Since plane-wave insonification is generally desired in panel tests, these results demonstrate the necessity of using a directional source in such tests, and illustrate the magnitude of the measurement errors that can result by using a nondirectional source such as the F56.

V. SUMMARY AND CONCLUSIONS

This article has presented the results of measurements that demonstrate that edge diffraction from a soft underwater acoustic panel can be observed by using measurements obtained from a carefully fabricated airbox. Two different source types and two different hydrophone-to-panel offset distances were considered. The validity of the edgewave measurements was established by demonstrating that the performance of a relatively small sample, as based on the frequency-by-frequency sum of edge-diffraction-free measurements from a relatively large sample plus measurements from the airbox sample, is in reasonably good agreement with direct measurements in the transmission region of the relatively small sample.

The results presented are directly useful for estimating edgewave contamination in panel measurements which approximate the conditions considered. The methods described could also be used to extend the results to other measurement geometries and techniques.[8]

ACKNOWLEDGMENTS

I am indebted to A. R. Garceau for his efforts in data acquisition as well as sample and rigging design and fabrication. This work was supported by the Office of Naval Research.

[1] R. J. Bobber, *Underwater Electroacoustic Measurements* (U.S. Government Printing Office, Washington, DC, 1970).
[2] A. J. Rudgers and C. A. Solvold, "Apparatus-independent acoustical-material characteristics obtained from panel-test measurements," J. Acoust. Soc. Am. **76**, 926–934 (1984).
[3] D. A. Sachs, "Edge diffraction effects in panel measurements," ONR/NUSC Symposium Proceedings on the Dynamic Mechanical Properties of Elastomers (Dept. of the Navy, Underwater Systems Center, New London, CT, 1984), pp. 222–223.
[4] J. C. Piquette, "An analytical technique for reducing the influence of edge diffraction in reflection measurements made on thin acoustical panels," J. Acoust. Soc. Am. **80**, 19–27 (1986).
[5] J. C. Piquette, "Technique for detecting the presence of finite sample-size effects in transmitted-wave measurements made on multilayer underwater acoustic panels," J. Acoust. Soc. Am. **90** 2831–2842 (1991).
[6] D. A. Sachs, "Edge diffraction interference in baffle performance measurements," J. Acoust. Soc. Am. Suppl. 1 **68**, S85 (1980).
[7] R. P. Radlinski, "Diffraction About an Acoustically Soft Panel," NUSC Technical Memorandum 801141 (1980).
[8] R. P. Radlinski, "Diffraction About Acoustically Soft Panels," NUSC Technical Document 8681 (1990).
[9] L. E. Ivey, *Underwater Electroacoustic Transducers* (USRD Transducer Catalog) (Naval Research Laboratory, Orlando, FL, Apr. 1992).
[10] I. D. Groves, "High Pressure Piezoelectric Ceramic Transducer," NRL Memorandum Report 6895 (Feb. 1969).
[11] J. C. Piquette, "Method for transducer transient suppression. I: Theory," J. Acoust. Soc. Am. **92**, 1203–1213 (1992).
[12] J. C. Piquette, "Method for transducer transient suppression. II: Experiment," J. Acoust. Soc. Am. **92**, 1214–1221 (1992).
[13] J. C. Piquette, "Spherical-wave scattering by a finite-thickness solid plate of infinite lateral extent, with some implications for panel measurements," J. Acoust. Soc. Am **83**, 1284–1294 (1988).
[14] J. C. Piquette, "Interactions of a spherical wave with a bilaminar plate composed of homogeneous and isotropic solid layers," J. Acoust. Soc. Am. **84**, 1526–1535 (1988).
[15] It is not yet possible to make a detailed comparison of theory and experiment for the spherical-wave case, since the sample holder plus sample combination actually forms a five-layer system, a case not considered in Refs. 13 and 14. The five-layer system arises from the fact that the large-sample holder includes two polycarbonate support sheets and is free-flooding. Thus the five layers of the system are polycarbonate, water, Microcell, water, and polycarbonate. Nonetheless, preliminary calculations based on the one- and two-layer theories described in Refs. 13 and 14 suggest that the differences between the F43 and F56 measurements reported here may not be due to the Microcell alone, but are very possibly caused by shear waves in the polycarbonate support sheets that arise under spherical-wave excitation.
[16] The maximum deflection at the center of the large sample due to the effects of buoyancy (measured with the help of an underwater video camera) was 4.2 cm. Thus it might be supposed that the large differences between the large-sample insertion-loss measurements for each of the two sources are attributable to effects associated with the nonplanar deformation of the sample. However, it is difficult to reconcile such an explanation with the facts that (i) the large-sample insertion-loss curves vary very slowly with hydrophone offset and (ii) the F56 insertion-loss curve does not fluctuate above and below the F43 curve as would be expected from interference, but rather always lies below the F43 curve. Both of these facts are consistent with the theory described in Refs. 13 and 14.
[17] It might be supposed that the edge-diffraction measurements as reported here are invalidated by the buoyancy displacements of the sam-

ıles. However, the hydrophone-to-panel offset for the small sample (the measurement of which was again effected by the use of an underwater video camera) was found to be 8.9 cm, indicating a buoyancy displacement of the small sample of 3.9 cm. The 8.9-cm hydrophone-to-panel offset for the small sample should be compared with the offset of 8.3 cm for the air-containing region of the airbox discussed previously. The 0.6-cm offset difference is expected to create only a very minor edge-wave amplitude error. This expectation is substantiated by the reasonable agreement between the solid and dot-dashed curves that are compared in Figs. 4(a) and (b) and 5(a) and (b). However, this 0.6-cm hydrophone offset difference between the small sample and airbox may explain some of the differences between the compared curves, especially at the upper end of the measured frequency interval, due to phase errors. Some of the differences are also attributable to phase errors associated with the 0.3-cm difference in buoyancy displacement (4.2 cm − 3.9 cm between the large and small samples and the 0.9-cm difference in buoyancy displacement (4.2 cm − 3.3 cm) between the large sample and the airbox.